

Experimental study of the Doppler shift generated by a vibrating scatterer

Régis Wunenburger,^{a)} Nicolás Mujica,^{b)} and Stéphan Fauve

Laboratoire de Physique Statistique, Ecole Normale Supérieure, CNRS UMR 8550, 24 rue Lhomond, 75231 Paris Cedex 05, France

(Received 9 May 2003; revised 28 October 2003; accepted 31 October 2003)

We report an experimental study of the backscattering of a sound wave of frequency f by a surface vibrating harmonically at frequency F ($F \ll f$) and amplitude A in the regime where the Doppler effect overcomes bulk nonlinear effects. When the duration t_0 of the analyzed time series of the scattered wave is small compared to the vibration period, the power spectrum of the backscattered wave is proportional to the probability density function of the scatterer velocity, which presents two peaks shifted from f by roughly $2fA\Omega/c$ ($\Omega = 2\pi F$). On the contrary, when $t_0 \gg F^{-1}$, sidebands at frequencies $f \pm nF$ (n integer) appear in the power spectrum, which are due to the phase modulation of the backscattered wave induced by its reflection on a moving boundary. We use the backscattered power spectrum to validate the phase modulation theory of the Doppler effect in the latter case for $2kA \ll 1$ and $2kA \geq 1$ ($k = 2\pi f/c$, where c is the wave velocity) and we test the validity of an acoustic nonintrusive estimator of A as a function of power spectrum bandwidth and of A itself. © 2004 Acoustical Society of America. [DOI: 10.1121/1.1635414]

PACS numbers: 43.20.Fn, 43.28.Py, 43.25.Lj [MFH]

Pages: 507–514

I. INTRODUCTION

Velocity measurement using the Doppler shift of a wave reflected from a moving object is a widely used technique both with electromagnetic and acoustic waves. For objects moving at constant velocity, it is well known that the Doppler shift, calculated by means of coordinate transformation, is proportional to the velocity. The problem is more difficult when the motion is time dependent. In the case of a periodically oscillating object the problem was first carefully studied for electromagnetic waves.¹ The spectrum of the scattered wave is also modified due to the Doppler effect, which can be understood either as a nonlinear boundary condition imposed by the moving object^{1,2} or as caused from the inhomogeneity in time of the moving medium that supports the wave propagation.³ More precisely, the spectrum of the wave at frequency f scattered by a sinusoidally oscillating surface at frequency F is similar to that of a phase modulation process,¹ i.e., sidebands at frequencies $f \pm nF$ (n integer) appear in the spectrum of the scattered wave.

In the case of acoustic scattering, the situation is more complex, as the oscillating scatterer also emits a sound wave at frequency F which interacts with the scattered wave due to the nonlinear character of the equations of sound propagation.^{4,5} Rogers remarked⁶ that the bulk nonlinear wave mixing produces the same sideband peaks in the spectrum of the backscattered sound wave as the Doppler effect. Due to the lack of any decisive experiment, the criteria al-

lowing us to discriminate between the two effects have been the subject of an intense debate,^{3,6–11} and it has even been claimed that the contribution of the Doppler effect might be undetectable.^{6,8–11} In a previous letter,¹² we showed that there exists a wide parameter range in which the Doppler shift gives the dominant contribution to the spectrum of the scattered wave and studied the cross-over to the bulk dominated nonlinear regime.

In this article we focus on the experimental situation where the Doppler effect induced by a vibrating scatterer overcomes bulk nonlinearities. In particular we study the backscattering of a high frequency f sound wave by a plane scatterer oscillating at low frequency $F \ll f$. We study the characteristic features of the Doppler effect in both the static and quasi-static regimes and we validate the phase modulation theory of the Doppler effect in the quasistatic regime for $2kA \ll 1$ and $2kA \geq 1$. Many studies have been devoted to vibration measurements using ultrasonic techniques.^{13–18} In particular, Huang *et al.* proposed an acoustic nonintrusive estimator of the scatterer oscillation amplitude based on the phase modulation of the backscattered wave.¹⁵ To our knowledge, this estimator has not been validated experimentally. By comparing the scatterer oscillation amplitude obtained with both the acoustic nonintrusive estimator and vibration measurements performed with an accelerometer, we verify the accuracy of Huang *et al.*'s amplitude estimator.

This paper is organized as follows: in Sec. II we present the conditions for observing the static and quasi-static Doppler effect, and we recall some predictions concerning both surface Doppler and bulk nonlinear effects. This helps us to justify our choice of the experimental configuration, which is presented in Sec. III. In Sec. IV we present the main features of the static and quasi-static Doppler effect. In Sec. V we finally test the validity of a nonintrusive estimator of the

^{a)}Permanent address: Center de Physique Moléculaire Optique et Hertzienne, Université Bordeaux I, 351 cours de la Libération, 33405 Talence Cedex, France. Electronic mail: r.wunenburger@cpmoh.u-bordeaux1.fr

^{b)}Permanent address: Departamento de Física, Facultad de Ciencias Físicas y Matemáticas, Universidad de Chile, Av. Blanco Encalada 2008, Santiago, Chile. Present address: Nonlinear Dynamics Laboratory, Institute for Research in Electronics and Applied Physics, Bldg 223, University of Maryland, College Park, MD 20742.

scatterer oscillation amplitude. Conclusions are given in Sec. VI.

II. THEORETICAL CONSIDERATIONS

A. Static versus quasi-static Doppler effect

The usual picture of the Doppler effect is the constant frequency shift of an incident or emitted wave by an object moving at constant velocity V , which we will call the static Doppler effect. In the case of backscattering, the frequency shift Δf encountered by the scattered wave of frequency f is $2fV/c$. From an experimental point of view, when the velocity of the scatterer varies, the latter approach remains valid when the timescale of velocity variations is much larger than the duration t_0 of the scattered wave time series which is analyzed. For a periodic motion of frequency F , this implies $t_0 \ll F^{-1}$. In this case, the statistical distribution of the successively measured Doppler shifts is proportional to the probability density function (PDF) of the object velocity. In practice, since f and F are not commensurate, the computed power spectrum of the backscattered wave is the average of power spectra of many successive signal time series of duration t_0 ($t_0 \gg f^{-1}$) measured at random phase of the scatterer motion. Thus, this time-averaged power spectrum is expected to be proportional to the PDF of the scatterer velocity.

When t_0 is large enough so that the scatterer velocity varies during the acquisition, an analysis in terms of modulation of the time of flight of the scattered wave shows that the wave is phase modulated. To show this, we will consider the unidimensional situation where a plane progressive monochromatic sound wave propagating at velocity c in a quiescent medium is backscattered by a plane scatterer. This object has an infinite acoustic impedance (normal total reflection) and oscillates sinusoidally around its mean position according to the trajectory $x_S(t) = A \sin \Omega t$. We assume that the wave is emitted at time $t - \tau(t)$ by a transducer located at a distance L from the scatterer. The backscattered wave is then detected by the same transducer at time t such that

$$\tau(t) = \frac{2}{c} \left[L - x_S \left(t - \frac{\tau(t)}{2} \right) \right]. \quad (1)$$

This modulation of the time of flight of the wave induces a phase modulation of the backscattered wave detected at a distance L from the scatterer, such that

$$p^D \propto \exp i \omega(t - \tau(t)), \quad (2)$$

where the superscript “ D ” denotes the Doppler contribution to the backscattered wave. If $A \ll L$, we have $\tau(t) \approx 2L/c$. In addition, if the velocity of the plate is small compared to the sound velocity c , $M \equiv A\Omega/c \ll 1$, substitution of $\tau(t) \approx 2L/c$ in the argument of the vibration amplitude x_S in (1) is justified and leads to an explicit approximate expression for $\tau(t)$. This gives a phase modulation of the form

$$\omega \tau(t) \approx \frac{2\omega}{c} \left[L - x_S \left(\frac{t-L}{c} \right) \right]. \quad (3)$$

This is what is called the quasi-static approximation of the Doppler effect. The detected wave then rewrites

$$p^D \propto \exp i \left[\omega t + 2kA \sin \Omega \left(t - \frac{L}{c} \right) \right], \quad (4)$$

where $k = \omega/c$ is the wave number of the high frequency incident acoustic wave. The generation of sideband peaks at pulsation $\omega \pm n\Omega$ (n integer) in the spectrum of the backscattered wave is evidenced when transforming the latter expression to

$$p^D \propto \exp i(\omega t) \sum_{n=-\infty}^{+\infty} J_n(2kA) \exp \left[in\Omega \left(t - \frac{L}{c} \right) \right], \quad (5)$$

where J_n is the Bessel function of n th order. The sideband peaks at frequency $f \pm nF$ ($F = \Omega/2\pi$) have their amplitude proportional to $|J_n(2kA)|$. For $2kA \ll 1$, $J_n(2kA) \sim (kA)^n/n!$, and the Doppler effect is considered as weak, i.e., the energy of the peak at frequency f in the spectrum of the backscattered wave is almost equal to the energy of the incident wave, and the leading sideband peaks are at frequency $f \pm F$. Note that the condition $M \ll 1$ implies two possible situations: the first is $F \ll f$, thus Eq. (5) is valid for any value of $2kA$ such that $2kA \ll f/F$; the second is $F \sim f$, thus $A\omega/c \sim A\Omega/c \ll 1$, and therefore Eq. (5) is restricted to $kA \ll 1$.

Finally, the general case of oblique incidence has been widely studied theoretically.^{1,3,7,19,20} If we define θ as the angle between the incident wave and the normal of the surface, the argument of the Bessel functions of the scattered wave [Eq. (5)] must be replaced by

$$2kA \rightarrow (k_z + k_{nz})A, \quad (6)$$

where $k_z = k \cos \theta$, $k = \omega/c$,

$$k_{nz} = \sqrt{\left(\frac{\omega + n\Omega}{c} \right)^2 - k_x^2}, \quad (7)$$

and $k_x = k \sin \theta$. The argument $(k_z + k_{nz})A$ depends then on n and θ . If $F \ll f$ and if we restrict to the first sidebands, we can approximate $(\omega + n\Omega)/c \approx \omega/c$ in (7). Thus, the argument of the Bessel functions results,

$$(k_z + k_{nz})A \approx 2kA \cos \theta, \quad (8)$$

and, for small angles, the multiplicative correction term is almost unity, $\cos \theta \approx 1 - \theta^2/2$. Thus, from an experimental point of view, a simple configuration to study is $\theta \ll 1$ and $F \ll f$; in this case, Eq. (5) holds for any value of $2kA$ such that $2kA \ll f/F$.

B. Surface quasi-static Doppler effect versus bulk nonlinear effects

Due to the intrinsic nonlinear character of the conservation equations and to the nonlinear dependence of pressure fluctuations against density fluctuations (as a consequence of the equation of state of the fluid), sound propagation is nonlinear.^{4,5} Thus, two collinear waves of frequencies f_1 and f_2 may interact and generate waves whose frequencies are linear combinations of f_1 and f_2 , and whose amplitudes increase with the distance of interaction L .⁵ Considering our experiment, the nonlinear interaction of the low frequency wave p_Ω emitted by the vibrating scatterer and the high frequency backscattered wave p_ω leads to the generation of

sideband peaks in the spectrum of the detected wave. In the case of weak nonlinear interaction, the amplitude of the first sideband is to leading order proportional to

$$p_{\omega \pm \Omega}^{NL} = \frac{\epsilon}{2\rho c^3} (\omega \pm \Omega) p_{\Omega} p_{\omega} L, \quad (9)$$

where $\epsilon = B/2A + 1$ is the usual nonlinear parameter of the medium^{5,21} (here A should not be confused with the vibration amplitude). For gases, $\epsilon = (\gamma + 1)/2$, with $\gamma = c_p/c_v$ the specific heat ratio.

Therefore, when an acoustic wave is scattered by a vibrating surface, both the surface Doppler effect and bulk non-linearities contribute to the generation of combination frequencies. However, it has been argued that the Doppler effect is practically always dominated by bulk non-linearities.^{6,8-11} In the case of plane waves, Piquette and Van Buren¹⁰ and later Bou Matar *et al.*¹⁸ predicted that when the dimensionless parameter

$$Y = \frac{p_{\omega \pm \Omega}^D}{p_{\omega \pm \Omega}^{NL}} = \frac{2\rho c^2 A}{\epsilon L p_{\Omega}} \quad (10)$$

is large (resp. small) compared to unity, the Doppler effect (resp. bulk nonlinear effect) is dominant. Note that in addition to the plane wave assumption, such that $p_{\Omega} = \rho c v_{\Omega}$, these studies use the approximation that the amplitude of the low frequency velocity field is given by the scatterer velocity, i.e., $v_{\Omega} \approx A\Omega$, obtaining $Y = \Lambda/\epsilon\pi L$, where $\Lambda = c/F$. Completing the experimental demonstration by Bou Matar¹⁸ of the existence of two asymptotic regimes, a Doppler dominant regime and a bulk nonlinearity dominant one, we showed in our previous experimental study¹² that the criterium $Y = 1$, expressed in its more general form Eq. (10), is quantitatively correct.²² In this article, we focus on the Doppler effect, and therefore we choose an experimental configuration where the condition $Y \gg 1$, as defined by Eq. (10), is verified.

III. EXPERIMENTAL SETUP

Figure 1 displays the experimental setup. The vibrating scatterer consists of a square flat piston made of PMMA, 17×17 cm and 10 mm thick, located at $x = 0$ say. It is driven sinusoidally by an electromechanical vibration exciter of Bruel & Kjaer (BK) 4808 type, at a frequency $F = 14$ Hz and amplitude $10^{-6} \text{ m} < A < 3.5 \times 10^{-3} \text{ m}$. An air coupled transducer ITC 9073, $d = 12$ mm in diameter, located at a distance $L = 28$ cm, generates a wave at frequency $f = 225$ kHz, incident on the vibrating plane with a small angle $\theta = 5^\circ$. It is driven by the source of a high frequency spectrum analyzer Agilent 3589 amplified by a NF Electronic Instruments 4005 power amplifier. The incident wave on the piston is in the far field, as $d^2/4\lambda \approx 23.5 \text{ mm} \ll L$. The backscattered wave is detected by another ITC 9073 transducer, also located at a distance L , and oriented with an angle $\theta = -5^\circ$. The displacement of the piston is controlled by a Wavetek 395 function generator. This sinusoidal electric signal is amplified by a BK 2712 power amplifier, and the displacement is of the form $x_s(t) = A \sin(\Omega t)$. We note that the vibration harmonics

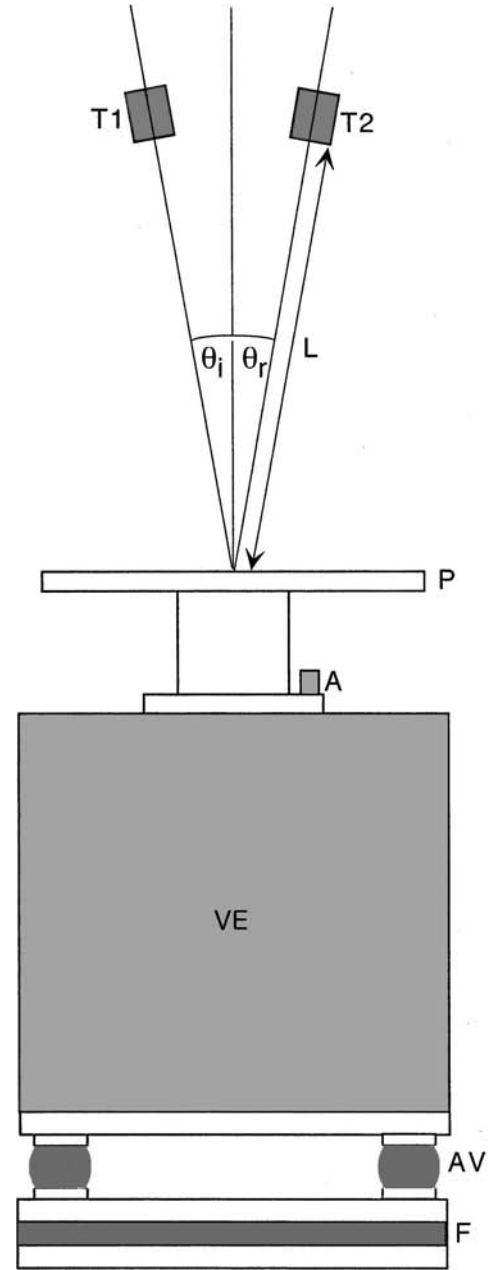


FIG. 1. Sketch of the experimental apparatus. (VE) electromechanical vibration exciter, (P) $17 \times 17 \times 1$ cm PMMA piston, (A) piezoelectric accelerometer, (T1-T2) air coupled transducers, (AV) anti-vibrations supports, and (F) foam anti-vibration layer. In the experiments described here, $\theta_i = \theta_r = \theta = 5^\circ$ and $L = 280$ mm. The piston displacement is $x_s(t) = A \sin(\Omega t)$.

have an energy at least 100 times smaller than the fundamental frequency vibration. The acceleration $-A\Omega^2 \sin(\Omega t)$ of the scatterer is measured using a BK 4393V piezoelectric accelerometer and a BK 2635 charge amplifier. The acceleration signal is processed using both an Agilent 35670A low frequency spectrum analyzer and a Stanford Research System 830 Lock-In amplifier, in order to get the displacement of the scatterer at F (the difference between both measurements is smaller than 0.5%). The power spectrum of the backscattered wave is computed with the high frequency Agilent 3589A spectrum analyzer. The experiment is controlled by a Power PC Mac computer and the data are transferred to this computer via a general purpose interface bus (GPIB) board.

Concerning the power spectrum measurements, an important parameter is $t_0 F$, where t_0 is the time duration of the analyzed time series, and t_0^{-1} is thus the spectral resolution (SR). In practice, it is the frequency span, f_{sp} , of the Agilent spectrum analyzer which is varied for a fixed number of points, $N=401$. Thus, $t_0^{-1}=f_{sp}/(N-1)$, and the frequency span takes the values 5 kHz, 2.5 kHz, 1.25 kHz, 625 Hz, and 312.5 Hz, giving $t_0^{-1}=12.5, 6.25, 3.125, 1.5625,$ and 0.78125 Hz.

Finally, in our experiment $\theta=5^\circ$ is finite but small. As discussed in Sec. II, if $F \ll f$ and if we restrict our analysis to the first sidebands, the argument of the Bessel functions appearing in Eq. (5) must be replaced by $2kA \cos \theta$ [see Eq. (8)]. This is indeed the case in our experiments, since $F \sim O(10 \text{ Hz})$, $f \sim O(225 \text{ kHz})$, and the number of analyzed sidebands is either 5 or 11. For $\theta=5^\circ$, the correct argument of the Bessel functions is $2kA \cos \theta \approx 1.992kA$, which represents a 0.4% error with respect to $2kA$. This error is small compared to the errors related to the measurements of A and the error on k (given by the approximation $c \approx 345 \pm 5$ m/s at 25°C), and it is then considered as negligible. Therefore, we simply use the parameter $2kA$ in the analysis of our experimental results.

IV. MAIN CHARACTERISTIC FEATURES OF THE DOPPLER EFFECT

A. Static Doppler effect

As explained above, when $t_0^{-1} \gg F$ the time averaged backscattered wave power spectrum is expected to be proportional to the PDF of the scatterer velocity. In addition, a static Doppler shift can be detected only if it exceeds the spectral resolution. This implies an additional condition, $2fA\Omega/c > t_0^{-1}$, i.e., $2kA \gg 1$. In our experimental setup both conditions are simultaneously verified for $F=5$ Hz and $A \geq 1.7$ mm. In addition $Y \gg 1$, and we are then in the Doppler dominated regime.

Figure 2(a) displays the backscattered wave power spectrum density (PSD) obtained for a low spectral resolution (SR) of $t_0^{-1}=12.5$ Hz, such that $t_0^{-1} \approx 2.5F$, and a scatterer vibration amplitude A verifying $2kA=32.6$. Thus, the conditions for observing a static Doppler shift are approximately verified. We observe that the spectrum displays two maxima, and we define Δf as the frequency shift of these maxima; in this case $\Delta f \approx 150$ Hz. These maxima can be identified with the two maxima of the scatterer velocity PDF occurring at $\pm A\Omega$. Its theoretical expression

$$\text{PDF}[\dot{x}_S/A\Omega] = \frac{1}{\pi \sin(\arccos(\dot{x}_S/A\Omega))} \quad (11)$$

is presented in Fig. 2(b) together with the experimental PDF of the actual scatterer velocity normalized by the value $A\Omega = 0.125$ m/s, obtained with the acceleration measurement done with the lock-in amplifier. Note that in Fig. 2(a) two pairs of extra symmetric peaks appear at roughly $2\Delta f$ and $3\Delta f$, but they are of much lower intensity. They probably correspond to the Doppler shifts of the waves which undergo multiple reflections on the scatterer.

Figure 3 displays the variations of Δf as a function of

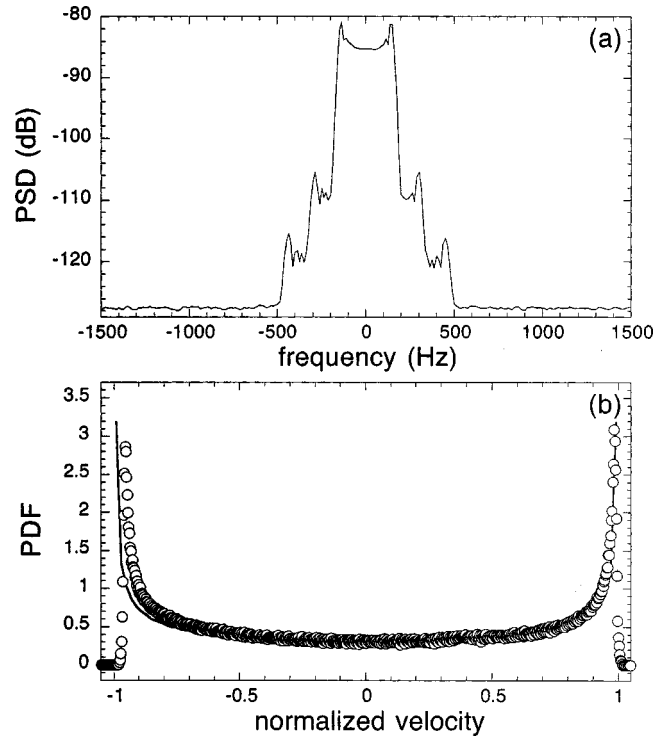


FIG. 2. (a) Backscattered wave power spectrum density (PSD) for $F=5$ Hz and $t_0^{-1}=12.5$ Hz. Frequencies are shifted by $f=225$ kHz. (b) Experimental (O) and theoretical (solid line) PDFs of the normalized scatterer velocity.

the expected static Doppler frequency shift $2fA\Omega/c$. The solid line represents the expected correlation between these two quantities in the static Doppler effect regime. The systematic underestimation of Δf is probably due to the fact that the scatterer velocity is not constant during the time of signal acquisition. Nevertheless, there is a satisfactory correlation between both quantities.

Figure 4 displays the backscattered wave power spectra

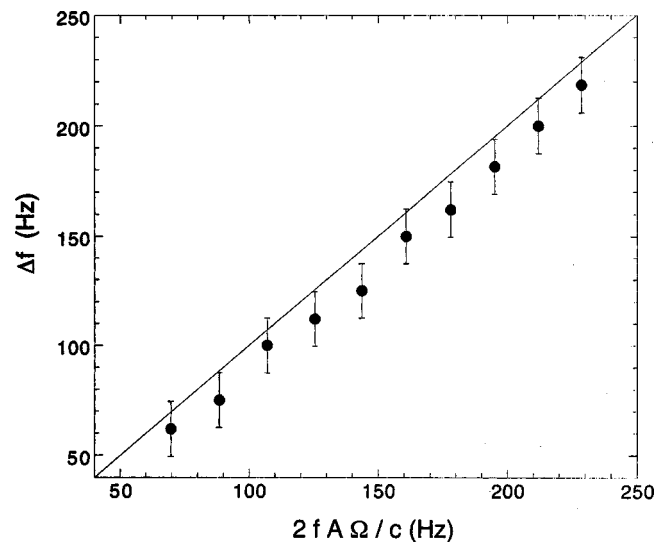


FIG. 3. Maximal frequency shift measured from the backscattered wave power spectrum Δf as a function of $2A\Omega f/c$ which is the expected static Doppler shift obtained from acceleration measurements. Error bars correspond to the frequency resolution $t_0^{-1}=12.5$ Hz and $F=5$ Hz. Solid line represents $\Delta f=2A\Omega f$.

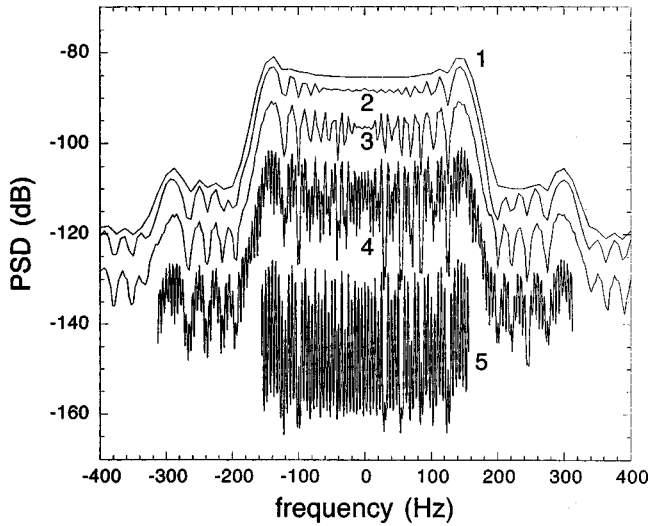


FIG. 4. Backscattered wave power spectra for $F=5$ Hz and $t_0^{-1}=12.5$ Hz (1), 6.25 Hz (2), 3.125 Hz (3), 1.5625 Hz (4), and 0.78125 Hz (5). Frequencies were shifted by $f=225$ kHz. Curves (3)–(5) have been shifted down by 5, 15, and 40 dB, respectively, for a better display.

obtained for various spectral resolutions ranging from $t_0^{-1} = 12.5$ to 0.78125 Hz. For a larger SR, $t_0^{-1} = 6.25$ Hz $\geq F$, the condition of static Doppler effect is not verified, and curve 2 of Fig. 4 displays several peaks between the two maxima of curve 1. The number of peaks increases with the spectral resolution (curves 3 and 4) until the frequency difference between two peaks drops to $F=5$ Hz (curve 5). As we explain in the following, this can be understood in the frame of the quasi-static Doppler effect presented in Sec. II. Note that whereas in the static Doppler effect regime the frequency difference between two peaks in the scattered wave power spectrum is determined by the scatterer oscillation *velocity amplitude*, in the quasi-static Doppler effect regime it is determined by the scatterer oscillation *frequency*.

B. Quasistatic Doppler effect

In this section we present experimental results concerning the quasi-static Doppler effect. We show that in our current experimental configuration, which is slightly different than in Ref. 12, the Doppler effect overcomes bulk nonlinearities in the generation of the sidebands at $f \pm nF$ of the backscattered wave. Although the prediction of the phase modulation theory concerning the amplitude of the first sideband is often used in the “weak regime” $2kA \ll 1$ in various applications,^{13–18} the phase modulation theory has never been experimentally verified, especially in the “strong regime” $2kA \geq 1$.

Three pressure power spectra of the backscattered wave computed for $f=225$ kHz, $F=14$ Hz, and three different values of the dimensionless amplitude $2kA$ are displayed in Fig. 5. (For the calculation of $k = \omega/c$ we used $c \approx 345$ m/s for air at ambient temperature $T_0 = 25 \pm 1$ °C.) These spectra are composed of pairs of symmetric peaks at $f \pm nF$ surrounding the central peak at f . Comparison of spectra 5a and b shows that the number of sidebands emerging from the background noise around the central peak at f increases with $2kA$, exceeding the frequency span for $2kA \geq 1$. A first can-

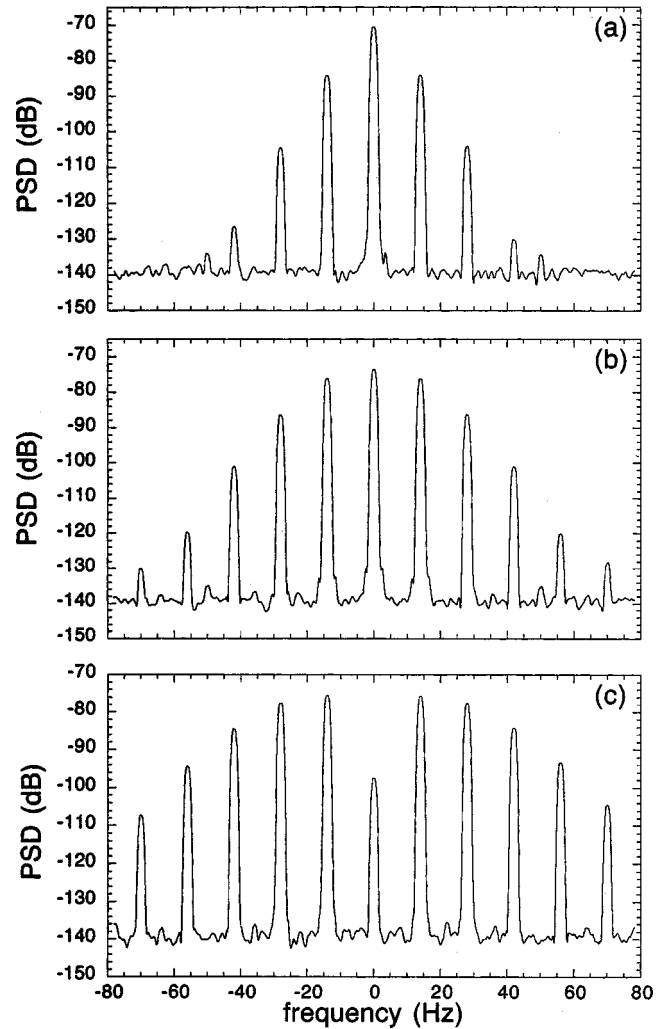


FIG. 5. Power spectra of the wave scattered by the vibrating plate as a function of the dimensionless vibration amplitude $2kA=0.39$ (a), 1.17 (b), and 2.34 (c) (k is the wave number of the incident wave of high frequency f). Frequencies were shifted by $f=225$ kHz. For the calculation of $k = \omega/c$ we used $c=345$ m/s for air at ambient temperature $T_0=25 \pm 1$ °C.

cellation of the central peak occurs at $2kA \approx 2.3$, as shown in Fig. 5(c), where the central peak has decreased by approximately 30 dB with respect to its initial value.

Figure 6 displays the variations of the normalized amplitudes $p_n = p_{\omega+n\Omega}/p_{\omega_0}$ of the sidebands measured in the power spectrum of the backscattered wave as a function of $2kA$, in both the weak (a), $2kA \ll 1$, and strong (b,c), $2kA \geq 1$, regimes. Normalization is done using the amplitude p_{ω_0} of the wave backscattered on the motionless piston (called hereafter the reference wave). Comparison with the predictions of phase modulation theory, i.e., with the absolute values of the Bessel functions, shows excellent agreement, except for high order sidebands when their amplitude is close to the background noise (this is for $p_n \lesssim -65$ dB, i.e., $p_n \lesssim 6 \times 10^{-4}$). For $2kA$ small, the amplitude of the sidebands at frequency $f \pm nF$ ($n=0-5$) increases like $(kA)^n/n!$. For higher values of $2kA$, the amplitude of the component at frequency f of the scattered wave decreases and we observe that it almost vanishes for $2kA \approx 2.3$ [see Figs. 5(c) and 6(b)]. It then increases when $2kA$ is increased further above 2.3, and then decreases and vanishes again for $2kA \approx 5.4$.

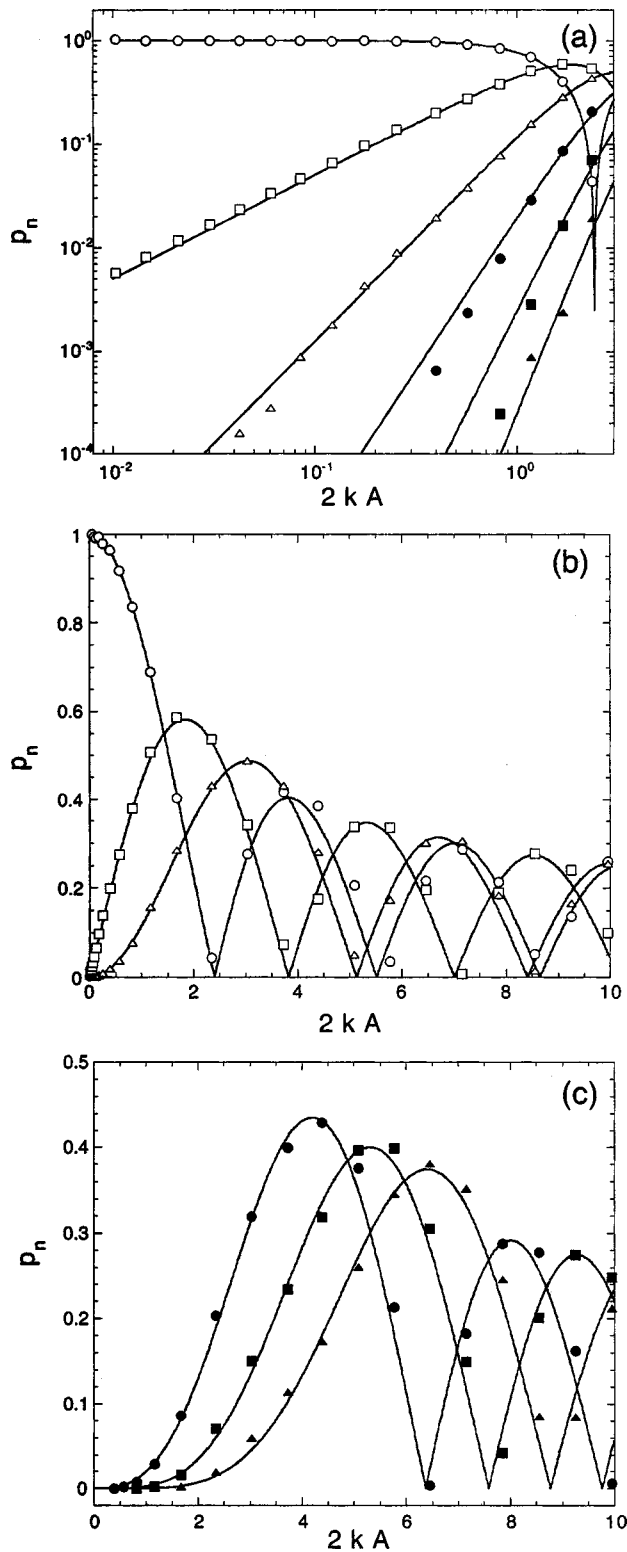


FIG. 6. Normalized pressure $p_n = p_{\omega+n\Omega} / p_{\omega_0}$ versus $2kA$ for $n=0$ (\circ), 1 (\square), 2 (\triangle), 3 (\bullet), 4 (\blacksquare), and 5 (\blacktriangle). p_{ω_0} is the amplitude of the wave backscattered on the motionless piston. (a) Weak regime in \log_{10} - \log_{10} scale and (b) and (c) strong regime in linear scale. Continuous lines show the absolute values of the Bessel functions of order $n=0, \dots, 5$. Note that there is no adjustable parameter, and k is fixed by the sound speed c .

The same process occurs roughly periodically for the amplitude of each peak $f \pm nF$, as displayed in Fig. 6 for $n=0-5$. We note that experiments were performed up to $2kA=30$, showing the same behavior.

Another way to check that the Doppler effect is dominant versus bulk acoustic nonlinearities is to vary the vibration frequency, always keeping $Y \gg 1$, and to show that the sideband amplitudes p_n scale like A , independently of F . This is indeed the case in our experimental configuration. Thus, the Doppler effect is the dominant mechanism in the generation of frequency combinations $f \pm nF$. We can then study an acoustic nonintrusive estimator of the vibration amplitude A , which is presented in the next section.

V. TEST OF A SPECTRAL ESTIMATOR OF THE SCATTERER HARMONIC VIBRATION AMPLITUDE

Recently, Huang *et al.*¹⁵ proposed to use a mathematical property of Bessel functions,

$$z = \sqrt{\frac{2 \sum_{n=-\infty}^{+\infty} n^2 J_n^2(z)}{\sum_{n=-\infty}^{+\infty} J_n^2(z)}}, \quad (12)$$

in order to define a spectral estimator \hat{A} of the scatterer vibration amplitude A when its motion is harmonic in the quasi-static Doppler regime. In practice, the number of detected sidebands being finite, the estimator has to be defined with a finite number of sidebands $2n_0$:

$$\hat{A} = \frac{1}{\sqrt{2}k} \sqrt{\frac{\sum_{n=-n_0}^{+n_0} n^2 p_n^2(2kA)}{\sum_{n=-n_0}^{+n_0} p_n^2(2kA)}}. \quad (13)$$

We can then test the accuracy and validity domain of this estimator. It is expected to be valid as long as the energy of the undetected sidebands is small compared to the energy of the detected ones. This can be checked by measuring the energy of the backscattered wave E and comparing it to the energy of the reference wave E_0 . As a matter of fact, due to the orthogonality of the Bessel functions, the normalized energy of a wave of the form given by Eq. (5) is

$$\frac{E}{E_0} = \sum_{n=-\infty}^{+\infty} J_n^2(2kA) = 1. \quad (14)$$

As long as the undetected energy is small compared to the one of the reference wave, we expect the estimator \hat{E} to be equal to the energy of the reference wave:

$$\hat{E} = \sum_{n=-n_0}^{+n_0} p_n^2(2kA) \approx E_0. \quad (15)$$

This reflects the fact that the phase modulation process induced by the scatterer vibration does not transfer any energy from the scatterer to the scattered wave. In fact, the energy of the sidebands is pumped from the incident wave only.

Figure 7(a) displays the average relative error $\hat{A}/A - 1$ as a function of $2kA$ for $n_0=5$ and 11, where A is determined from the scatterer acceleration. The averages are performed over 22 independent experimental runs for each value of A . This average relative error is compared to the error computed using a theoretical truncated amplitude estimator \hat{A}_T , which is defined with the finite number of detected sidebands:

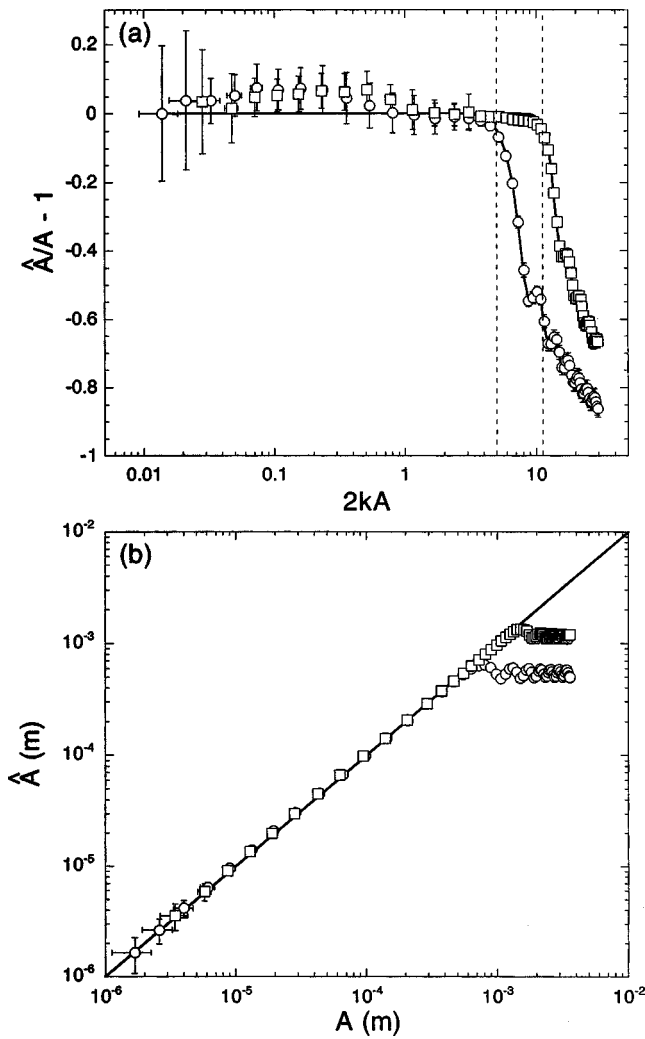


FIG. 7. (a) Amplitude estimator error, $\hat{A}/A - 1$, versus $2kA$. The solid line represents the theoretical truncated amplitude estimator error. Vertical dashed lines represent the values $2kA = n_0$. Error bars correspond to the errors obtained including the standard deviation of 22 independent experimental runs, the errors associated to the amplitude measurements, and the error associated to the value of k ($\pm 1.5\%$ for c). (b) Estimated amplitude \hat{A} versus A . In this case the error bars correspond to the statistical standard deviation of 22 independent experimental runs. In both figures, results for two PSD spans are presented, $n_0 = 5$ (\circ) and 11 (\square).

$$\hat{A}_T = \frac{1}{\sqrt{2k}} \sqrt{\frac{\sum_{n=-n_0}^{+n_0} n^2 J_n^2(2kA)}{\sum_{n=-n_0}^{+n_0} J_n^2(2kA)}}. \quad (16)$$

In the range $2kA < n_0$, the estimator \hat{A} , defined in Eq. (13), is found to have a satisfactory accuracy. The mean value of $\hat{A}/A - 1$ does not exceeds 5%. The associated errorbars are important (of the order of 20%) for $2kA \approx 0.01$, but they decrease rapidly to a value below 5% as we increase A . The larger errors are in fact due to the uncertainty of the determination of the amplitude from acceleration measurements at low frequency (At both low F and low A , the acceleration is quite small, of the order of $1.6 \times 10^{-2} \text{ m/s}^2$.) However, the relative errors of both amplitude measurements, i.e., the acceleration and nonintrusive acoustic power spectrum estimator measurements, are of same order of mag-

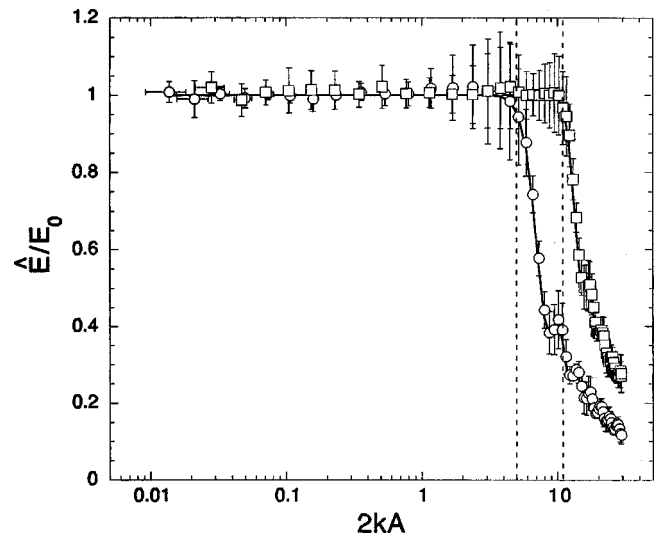


FIG. 8. Estimated normalized acoustic energy \hat{E}/E_0 versus $2kA$ for two PSD spans, $n_0 = 5$ (\circ) and 11 (\square). In this case the errorbars correspond only to the standard deviation of 22 independent experimental runs. Vertical dashed lines represent the values $2kA = n_0$.

nitude, as can be seen in Fig. 7(b), where we present \hat{A} versus A in a $\log_{10} - \log_{10}$ scale.

In Fig. 7(a) we observe that for $n_0 = 5$ (resp. 11) the estimation error increases above 5% when $2kA > 5$ (resp. 11), in agreement with the error computed using the theoretical truncated amplitude estimator $\hat{A}_T/A - 1$. This departure from 0 is concomitant with the saturation of \hat{A} observed in Fig. 7(b). These facts are due to the transfer of a significant part of the incident energy to undetected sidebands during scattering. This is clearly observed in Fig. 8, which shows the average value of \hat{E}/E_0 as a function of $2kA$. It is compared to the normalized energy computed using a theoretical truncated energy estimator \hat{E}_T/E_0 , defined as

$$\frac{\hat{E}_T}{E_0} = \sum_{n=-n_0}^{+n_0} J_n^2(2kA). \quad (17)$$

Here, we also find that both \hat{E}/E_0 and \hat{E}_T/E_0 drop by more than 5% when $2kA > n_0$.

We thus conclude that for the experimental configuration presented here, the acoustic amplitude estimator proposed in Ref. 15 is valid in a large range of amplitudes, namely $2 \times 10^{-2} < 2kA < n_0$, which gives $2 \times 10^{-3} \text{ mm} < A < n_0/2k \approx 1.2 \text{ mm}$ (resp. 2.7 mm) for $n_0 = 5$ (resp. $n_0 = 11$). The relative error on \hat{A} is of the same order of magnitude as that on the acceleration measurements. The lower limit of A is given by the signal-to-noise ratio (SNR) of the acceleration measurements whereas the lower limit of \hat{A} is given by the PSD SNR, which is of the order of 65 dB in our present experimental configuration. Concerning the acoustic nonintrusive estimator \hat{A} , for small amplitude measurements ($2kA \ll 1$) the first sidebands must then satisfy $p_{\omega \pm \Omega}/p_{\omega 0} = p_1/p_0 \approx kA > -65 \text{ dB} \approx 6 \times 10^{-4}$ in order to be resolved. Thus, to get a better resolution on the measured amplitude we have to increase k , i.e., to increase f .²³ On the other hand, to increase the upper limit of the measurable amplitude, one has to in-

crease the ratio n_0/k , either by increasing the number of sidebands taken into account in the analysis or by decreasing k (by decreasing f).

VI. CONCLUSION

We have studied the Doppler effect generated by vibrating scatterers. We have shown that depending on the duration t_0 of the analyzed backscattered wave, we have two possible situations: (i) if $t_0 \ll F^{-1}$, the static Doppler effect is observed and the backscattered power spectrum is proportional to the PDF of the scatterer velocity. The frequency shift Δf is then given by the amplitude of the scatterer velocity. (ii) If $t_0 \gg F^{-1}$, the so-called quasi-static Doppler effect is observed, and the scattered wave is phase modulated by the normalized vibration displacement $2kx_s(t) = 2kA \sin(\Omega t)$. In this case, the backscattered wave has a frequency spectrum composed of peaks at $f \pm nF$ (n integer). Experiments show that the backscattered wave is very well described by Eq. (5), i.e., the amplitudes of the sidebands of order n are given by the Bessel functions of order n . We verified that in the case $F \ll f$, this agreement holds in both the weak ($2kA \ll 1$) and strong ($2kA \geq 1$) regimes.

The last part of this work was devoted to the study of a noninvasive acoustic estimator of the amplitude vibration A . We conclude that for the present experimental configuration, the acoustic amplitude estimator is valid for a large range of amplitudes, namely $2 \times 10^{-2} < 2kA < n_0$, which gives $2 \times 10^{-3} \text{ mm} < A < n_0/2k \approx O(1 \text{ mm})$. To increase the upper bound one has to take into account a larger number of sidebands or one can choose to decrease the incident sound frequency. For a given SNR, one has to increase the incident frequency to decrease the lower bound.

ACKNOWLEDGMENTS

RW thanks the Center National d'Etudes Spatiales (CNES) for financial support. This work has been supported by CNES Contract No. 03/11/21/00.

¹A. M. Kovalev and V. N. Krasil'nikov, "Reflection of electromagnetic waves from moving surfaces," *Sov. Phys. Tech. Phys.* **7**, 19 (1962).

²D. Censor, "Scattering by time varying obstacles," *J. Sound Vib.* **25**, 101–110 (1972).

³D. Censor, "Acoustical Doppler effect analysis—Is it a valid method?" *J. Acoust. Soc. Am.* **83**, 1223–1230 (1988).

⁴M. F. Hamilton and C. L. Morfey, "Model equations," in *Nonlinear Acoustics*, edited by M. F. Hamilton and D. T. Blackstock (Academic, New York, 1998).

⁵K. Naugolnykh and L. Ostrovsky, *Nonlinear Wave Processes in Acoustics* (Cambridge U.P., Cambridge, 1998).

⁶P. H. Rogers, "Comments on 'Scattering by time varying obstacles,'" *J. Sound Vib.* **28**, 764–768 (1973).

⁷D. Censor, "Harmonic and transient scattering from time varying obstacles," *J. Acoust. Soc. Am.* **76**, 1527–1534 (1984).

⁸J. C. Piquette and A. L. Van Buren, "Nonlinear scattering of acoustic waves by vibrating surfaces," *J. Acoust. Soc. Am.* **76**, 880–889 (1984).

⁹J. C. Piquette and A. L. Van Buren, "Comments on Harmonic and transient scattering from time varying obstacles [*J. Acoust. Soc. Am.* **76**, 1527–1534 (1984)]," **79**, 179–180 (1986) and author's reply.

¹⁰J. C. Piquette and A. L. Van Buren, "Some further remarks regarding scattering of an acoustic wave by a vibrating surface," *J. Acoust. Soc. Am.* **80**, 1533–1536 (1986).

¹¹J. C. Piquette, A. L. Van Buren, and P. H. Rogers, "Censor's acoustical Doppler effect analysis—Is it a valid method?" *J. Acoust. Soc. Am.* **83**, 1681–1682 (1988).

¹²N. Mujica, R. Wunenburger, and S. Fauve, "Scattering of a sound wave by a vibrating surface," *Eur. Phys. J. B* **33**, 209–213 (2003).

¹³M. Cox and P. H. Rogers, "Automated noninvasive motion measurement of auditory organs in fish using ultrasound," *J. Vib. Sound Str. Rel. Design* **109**, 55–59 (1987).

¹⁴R. M. Lerner, K. J. Parker, J. Holen, R. Gramiak, and R. C. Waag, "Sonoelasticity: medical elasticity images derived from ultrasound signals in mechanically vibrated targets," *Acoust. Imaging* **16**, 31–37 (1988).

¹⁵S. Huang, R. M. Lerner, and K. J. Parker, "On estimating the amplitude of harmonic vibration from the Doppler spectrum of reflected signals," *J. Acoust. Soc. Am.* **88**, 2702–2712 (1990).

¹⁶Y. Yamakoshi, J. Sato, and T. Sato, "Ultrasonic imaging of internal vibration of soft tissue under forced vibration," *IEEE Trans. Ultrason. Ferroelectr. Freq. Control* **37**, 45–53 (1990).

¹⁷F. Figueroa and E. Barbieri, "An ultrasonic ranging system for structural vibration measurements," *IEEE Trans. Instrum. Meas.* **40**, 764–769 (1991).

¹⁸O. Bou Matar, J. P. Remenieras, C. Bruneau, A. Roncin, and F. Patat, "Noncontact measurement of vibration using airborne ultrasound," *IEEE Trans. Ultrason. Ferroelectr. Freq. Control* **45**, 626–633 (1998).

¹⁹L. M. Lyamshev, "Diffusion of sound by a periodically moving plate," *Sov. Phys. Dokl.* **28**, 274–276 (1983).

²⁰L. M. Lyamshev, "Distinctive features of the scattering and radiation of sound by periodically moving plates and shells," *Sov. Phys. Acoust.* **30**, 237–238 (1984).

²¹R. T. Beyer, "The parameter B/A ," in *Nonlinear Acoustics*, edited by M. F. Hamilton and D. T. Blackstock (Academic, New York, 1998).

²²The Doppler effect can dominate nonlinear effects for $Y < 1$ in the case of diverging waves because of a less efficient nonlinear interaction in the bulk whereas the Doppler effect remains unchanged.¹² The opposite effect is expected for converging waves.

²³For example, for experiments in water presented in Ref. 12, where the SNR is 80 dB, $L = 20$ cm, $F = 120$ Hz, and $f = 2.25$ MHz, using only one sideband, $n_0 = 1$, and for a single experimental run, we find that the relative error $\hat{A}/A - 1$ is lower than 15% for $7 \times 10^{-9} \text{ m} < A < 5 \times 10^{-5} \text{ m}$. Smaller errors can be obtained by averaging over several experimental runs as is done the present work.